

# We are IntechOpen, the world's leading publisher of Open Access books Built by scientists, for scientists

6,900

Open access books available

185,000

International authors and editors

200M

Downloads

Our authors are among the

154

Countries delivered to

TOP 1%

most cited scientists

12.2%

Contributors from top 500 universities



WEB OF SCIENCE™

Selection of our books indexed in the Book Citation Index  
in Web of Science™ Core Collection (BKCI)

Interested in publishing with us?  
Contact [book.department@intechopen.com](mailto:book.department@intechopen.com)

Numbers displayed above are based on latest data collected.  
For more information visit [www.intechopen.com](http://www.intechopen.com)



# Internal Waves Radiation by a Turbulent Jet Flow in a Stratified Fluid

Oleg Druzhinin

*Institute of Applied Physics, Russian Academy of Sciences  
Russia*

## 1. Introduction

The radiation of internal gravity waves by stratified turbulent shear flows is encountered in many geophysical flows. Numerous applications include jet flows (Sutherland & Peltier 1994), grid-generated turbulence (Dohan & Sutherland 2003), boundary layers (Taylor & Sarkar 2007), collapse of mixed patches (Sutherland et al. 2007), wakes behind towed and self-propelled bodies (Lin & Pao 1979), and many others. The present paper deals with internal waves radiated by a jet flow that is created in the far wake of a sphere towed in a stratified fluid at large Froude and Reynolds numbers.

Experimental studies of internal gravity waves (IW) radiated by a towed sphere and its wake were performed both in a linearly stratified fluid by Bonneton, Chomaz & Hopfinger (1993) (further referred to as BCH) and in the presence of a thermocline by Robey (1996). The results show that internal waves radiated by the sphere (i.e. the lee waves) are stationary with respect to the sphere, and their amplitude is inversely proportional to the sphere Froude number, defined as  $Fr = 2V / ND$  (where  $N$  is the buoyancy frequency, and  $V$  and  $D$  are the towing speed and the sphere diameter). On the other hand, internal waves, radiated by the turbulent wake are not stationary with respect to the sphere, and their amplitude grows as  $Fr$  increases. Experimental results obtained by BCH and Robey (1996) show that if the Froude number is sufficiently large ( $Fr > 10$ ), non-stationary IW supercede the lee waves.

Experimental results obtained by BCH show that at early times ( $Nt = O(10)$ ) internal waves are radiated due to the collapse of the vortex coherent structures developing in the near wake (Chomaz, Bonnet & Hopfinger (1993), further referred to as CBH). The wavelength of these waves (also called “random” waves) is of the order of the sphere diameter, and their dynamics is well described theoretically under an assumption that each collapsing coherent structure can be regarded as an impulsive source of IW. Visualization of the density distribution in a horizontal plane at a distance of three sphere radii below the towing axis at times  $Nt < 40$  gives a rather complicated, irregular isophase pattern of these random internal waves.

The results of BCH show also that at later times ( $Nt > 40$ ) random internal waves are superceded by waves whose initial spatial period is of the order of five sphere diameters. The isophase distribution of these waves, although being non-stationary with respect to the sphere, is reminiscent of the regular iso-phase pattern of the lee-waves. At sufficiently late times ( $Nt > 50$ ), the random waves disappear, and there remain only coherent IW. BCH give no explanation of the observed dynamics of these coherent internal waves.

The experimental study of internal waves produced by a sphere towed under a thermocline at large Froude and Reynolds numbers was performed by Robey (1996). The results also show that the turbulent wake generates coherent internal waves which are non-stationary with respect to the sphere and whose amplitude grows linearly with  $Fr$ . In order to explain these experimental observations Robey (1996) considers a physical model of the IW radiation by the wake. According to this model, internal waves are emitted by vortices shed by the sphere, and each vortex can be regarded as a stationary source moving at a “resonance” speed, such that its effective Froude number is of order unity. Note however, that experimental results obtained by CBH do not support the assumption that such stationary vortices are present in the near wake.

Another theoretical model of IW radiation by the wake flow has been developed by Dupont & Voisin (1996). According to this model, internal waves are emitted by an oscillating source moving with the speed of a sphere. It is assumed that such a source adequately represents coherent vortex structures which are shed by the sphere at the frequency of a spiral instability mode of the near-wake flow (observed experimentally by CBH) and collapse under gravity. Dupont & Voisin (1996) performed numerical calculations based on the Green’s function formalism developed by Voisin (1994). However, numerical results of Dupont & Voisin (1996) show that the IW phase pattern predicted by the model is rather complicated and does not reproduce the regular phase distribution related to the coherent internal waves observed experimentally by BCH.

Recently there have been successful attempts to perform DNS and LES of stratified wakes by Gourlay et al. (2001), Dommermuth et al. (2002) and Brucker & Sarkar (2010). Since the mean streamwise fluid velocity in the wake is much smaller than the sphere towing speed, the variation of the flow statistical properties along the streamwise ( $x$ ) axis can be neglected in DNS in the considered flow region. Thus the flow in DNS/LES is initialized as a sum of a circular, mean streamwise velocity profile and an  $x$ -periodic, random velocity component accounting for the turbulent fluctuations. This turbulent component is prescribed as a sum of Fourier harmonics with independent random phases and given amplitude power spectrum. Numerical results of Gourlay et al. (2001) (such as the temporal development of the wake axis mean velocity, width and height and the instantaneous vorticity distribution) are in good qualitative agreement with the experimental data obtained by Spedding et al. (1996) and Spedding (2001). Dommermuth et al. (2002) performed the LES study of the stratified wake and used a relaxation procedure to bring to equilibrium the initially unrelated turbulent production and dissipation. Their results are similar to the results of Gourlay et al. (2001) and show that the relaxation procedure is essential for accurately simulating the near wake but is not important if only far wake is of interest. DNS of the turbulent wake flow at high Reynolds number ( $Re=50000$ ) was performed recently by Brucker & Sarkar (2010) using the same flow initialization procedure. Both Gourlay et al. (2001) and Dommermuth et al. (2002) and Brucker & Sarkar (2010) conclude that stratified wakes are capable of radiating internal waves, but do not examine in detail the physical mechanism of the IW radiation and the properties of waves kinematics and dynamics. The radiation of internal waves by a turbulent jet flow in a linearly stratified fluid was studied recently by performing DNS by Druzhinin (2009). The results show that IW radiation occurs at times  $10 < Nt < 30$  and can be described as a result of an impulsive collapse of the vertical velocity fluctuation of the initially 3D turbulent flow.

The objective of the present paper is to study in more details the process of internal waves radiation by a temporally developing turbulent jet flow in a stratified fluid by direct numerical simulation. An initially circular, turbulent jet flow is considered with parameters

that match parameters of a far wake of a sphere towed in a stratified fluid at large Froude and Reynolds numbers (of order  $O(10)$  and  $O(10^4)$ , respectively). The mathematical formulation and description of the numerical procedure are provided in Section 2. In Section 3 the properties of the jet flow and radiated internal waves obtained in DNS are described. In Section 4 a linear impulsive source theory is applied to explain the observed IW kinematics and dynamics, and final conclusions are found in Section 5.

## 2. Governing equations and numerical method

A circular jet flow with the initial (reference) Gaussian profile of the streamwise ( $x$ ) velocity component is considered in the form:

$$U_{ref} = \exp\left(-4[y^2 + z^2]\right), \quad (2.1)$$

where  $y$  and  $z$  are the spanwise and vertical coordinates, respectively. Hereafter, all the variables are made dimensionless via normalizing by the velocity and length scales defined by the initial jet axis mean velocity and diameter,  $U_0$  and  $L_0$ . For example, in the case of a wake created by a towed sphere,  $L_0$  is close to the sphere diameter ( $L_0 / D \approx 0.8$ ) and  $U_0$  is defined by the towing speed  $V$  and the velocity deficit at the wake central axis at a given distance behind the sphere, e.g.  $U_0 / V \approx 0.1$  at  $x / D = 6$  (cf. Bevilaqua & Likoudis 1978). An initial linear, stable stratification of the fluid density is considered ( $\rho_{ref} = -z$ ). The Navier – Stokes equations for the fluid velocity are written under the Boussinesq approximation in the dimensionless form:

$$\begin{aligned} \partial_t U_i + U_j \partial_j U_i + U_{ref} \partial_x U_i + \delta_{ix} (U_y \partial_y U_{ref} + U_z \partial_z U_{ref}) = \\ -\partial_i P + \frac{1}{Re} \partial^2 U_i + \frac{1}{Re} \delta_{ix} (\partial_{yy}^2 U_{ref} + \partial_{zz}^2 U_{ref}) - \delta_{iz} Ri \rho, \end{aligned} \quad (2.2)$$

$$\partial_j U_j = 0. \quad (2.3)$$

The equation for the fluid density is written as:

$$\partial_t \rho + U_j \partial_j \rho + U_{ref} \partial_x \rho - U_z = \frac{1}{RePr} \partial^2 \rho. \quad (2.4)$$

In Eqs. (2.2) – (2.4),  $U_i$  ( $i = x, y, z$ ) and  $\rho$  are the instantaneous deviations of the fluid velocity and density from their respective reference profiles, and  $\delta_{ij}$  is the Kroneker's symbol. The Reynolds number and the global Richardson number of the flow are defined as:

$$Re = \frac{U_0 L_0}{\nu}, \quad (2.5)$$

and

$$Ri = \frac{g \Delta \rho_0}{\rho_0} \frac{L_0}{U_0^2}, \quad (2.6)$$

where  $\nu$  is the fluid kinematic viscosity,  $g$  the acceleration due to gravity, and  $(\Delta\rho_0/\rho_0)$  the absolute relative density variation in the vertical direction on scale  $L_0$ . (Note that since  $U_0/V \approx 0.1$ , the Reynolds and Froude numbers of the sphere are about 10 times larger than  $Re$  and  $Fr = Ri^{-1/2}$ , respectively.) As follows from eqs. (2.2) - (2.6), the dimensionless buoyancy frequency equals  $N = Ri^{1/2} = 1/Fr$ . The Prandtl number is set equal to unity. The results of DNS by Stadler et al. (2010) performed recently show that that  $Pr = 1$  is a reasonable approximation for  $Pr = 7$  which is the case of the thermal stratification in the ocean.

In order to perform numerical simulation in a region finite over the vertical coordinate and provide a sufficient resolution of the flow field, a mapping for the  $z$ -coordinate is employed in the form:

$$\xi = \tanh \frac{z}{9}, \quad (2.7)$$

so that

$$z = 4.5 \ln \left( \frac{1+\xi}{1-\xi} \right), \quad (2.8)$$

and  $-1 \leq \xi \leq 1$  for  $-\infty < z < \infty$ . The derivatives over  $z$ -coordinate in Eqs. (2.2)-(2.4) are rewritten as:

$$\frac{\partial}{\partial z} = \left( \frac{1-\xi^2}{9} \right) \frac{\partial}{\partial \xi}. \quad (2.9)$$

Equations (2.2) - (2.4) are discretized in a parallelepiped domain with sizes  $0 \leq x \leq 36$ ,  $-9 \leq y \leq 9$  and  $-1 \leq \xi \leq 1$  by employing a finite difference method of the second-order accuracy on a uniform rectangular staggered grid consisting of  $480 \times 240 \times 240$  nodes in  $x$ ,  $y$ , and  $\xi(z)$  directions, respectively. The terms on the left hand side of equations (2.2) and (2.4),  $U_{ref} \partial_x U_i$  and  $U_{ref} \partial_x \rho$ , that are responsible for the advection by the reference velocity  $U_{ref}(y, z)$ , are evaluated at each time step by Fourier interpolation which is a more accurate method to compute these terms as compared to a pure finite difference scheme (Gerz et al. (1989)). The integration is advanced in time using the Adams-Bashforth method with time step  $\Delta t = 0.0075$ . The shear-free (Neumann) boundary condition is prescribed in the spanwise and vertical directions (at  $y = \pm 9$  and  $\xi = \pm 1$ ), and  $x$ -periodic boundary condition is prescribed in the streamwise direction. The Poisson equation for the pressure is solved by fast Fourier transform over  $x$ -coordinate, cosine transform over  $y$ -coordinate, and Gauss elimination method over  $z$ -coordinate.

As it was observed by Goulet et al. (2001) in their DNS study, internal waves radiated by the jet turbulence propagate away from the jet core toward the boundaries of the computational domain in the  $y$  and  $z$  directions. Thus one needs to avoid reflection of the waves from the boundaries and their coming back into the flow region. One way to do this is to prescribe the Sommerfeld radiation boundary condition (cf. e.g. Javam et al. 2000). In the present study we adopt a less computationally expensive approach analogous to that employed by Sutherland & Peltier (1994) in their numerical study of the instability

development and IW radiation in a two-dimensional jet flow. In this approach, the absorption of internal waves radiated from the jet core is ensured by increasing the fluid kinematic viscosity in a layer near the boundaries of the computational domain. A similar viscous-sponge boundary condition was successfully employed recently by Taylor & Sarkar (2007) in their LES study of internal waves radiated by a turbulent boundary layer. Thus, in our DNS procedure the viscosity is increased by a factor of 20 in the region  $|y^2 + z^2|^{1/2} > 7$ , as compared to the viscosity in the rest of the computational domain (where it is constant and equals  $1/\text{Re}$ ). Our DNS results show that such artificial viscosity enhancement does not affect the jet flow dynamics and ensures complete absorption of internal waves radiated from the jet core region toward the boundaries. In order to define the flow statistical characteristics at a given time moment ( $t$ ), the  $x$  - averaged velocity and density fields are evaluated as:

$$\langle U_i \rangle (y, z, t) = \frac{1}{L_x} \int_0^{L_x} U_i(x, y, z, t) dx + \delta_{ix} U_{ref}(y, z), \quad (2.10)$$

$$\langle \rho \rangle (y, z, t) = \frac{1}{L_x} \int_0^{L_x} \rho(x, y, z, t) dx, \quad (2.11)$$

where  $i = x, y, z$ , and  $L_x = 36$ . The jet maximum mean velocity ( $U_m$ ) and its width and height ( $L_{y,z}$ ) are further evaluated as:

$$U_m(t) = \max\{\langle U_x \rangle (y, z, t)\}, \quad (2.12)$$

$$L_y(t) = \frac{1}{U_m} \int_{-\infty}^{\infty} \langle U_x \rangle (y, z = 0, t) dy, \quad (2.13)$$

$$L_z(t) = \frac{1}{U_m} \int_{-\infty}^{\infty} \langle U_x \rangle (y = 0, z, t) dz. \quad (2.14)$$

The instantaneous r.m.s. fluctuations of the velocity and density fields,

$$U'_i(y, z, t) = \langle U_i^2 - \langle U_i \rangle^2 \rangle^{1/2} \quad (2.15)$$

and

$$\rho'(y, z, t) = \langle \rho^2 - \langle \rho \rangle^2 \rangle^{1/2}, \quad (2.16)$$

and their amplitudes (the respective absolute maxima) are also evaluated.

The initial, random component of the fluid velocity is prescribed as a 3D homogeneous isotropic turbulence field consisting of a sum of Fourier harmonics with independent random phases and an isotropic amplitude power spectrum (Gourlay et al. 2001). We prescribe the initial turbulence spectrum to be uniform over the wavenumber range  $0.5 \leq k \leq 5$  and equal to zero for other  $k$ 's (Fig. 1). Thus, the initial spectrum includes the



most unstable (spiral) mode with  $k = 1.46$  of an inviscid non-stratified circular jet flow (Batchelor and Gill 1962), as well as a higher- $k$  axisymmetrical Kelvin-Helmholtz instability mode similar to that observed in the near wake flow (CBH 1993).

At present it is an open question whether the spiral shedding mode observed in the near wake (CBH 1993) is related to the spiral instability mode of the  $x$ -periodic circular jet, although the Strouhal numbers of the two modes are close (for the spiral mode  $St = k/2\pi = 0.2$  whereas for the shedding spiral mode  $St = 0.175$ , CBH 1993). It is possible that the two modes are related due to some correlation between the development of the instability of the near-wake flow and the location of the separation point of the boundary layer at the sphere and the development of the spiral shedding mode. It is important to note however that the development of the spiral instability mode is an intrinsic property of the circular jet/wake flow itself and not related to presence of the sphere.

Since at present there is no knowledge concerning the shape of the spectrum in the homogeneous near wake, we prescribe an initial uniform-amplitude spectrum. The initial amplitude of the random velocity component is prescribed to be about 40% of the mean velocity maximum. This value is close to the turbulence intensity measured by Bevilaqua and Lykoudis (1978) in a homogeneous turbulent wake at the distance  $x/D = 6$  behind the sphere. The initial velocity field is further windowed with the reference profile  $U_{ref}(y, z)$  (2.1) and made divergence-free, similarly to the initialization procedure employed by Gourlay et al. (2001).

The initial deviation of the density from the reference linear profile is prescribed to be zero. This is in agreement with the experimental observations of BCH showing that the effect of the turbulent mixing in the near wake of a towed sphere is weak and its contribution to the radiated IW field is negligible.

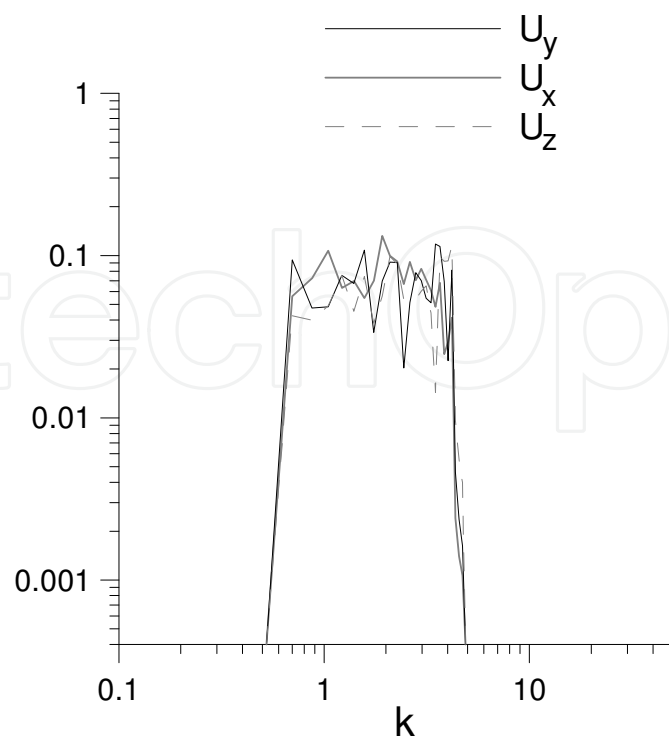


Fig. 1. The initial velocity spectrum.

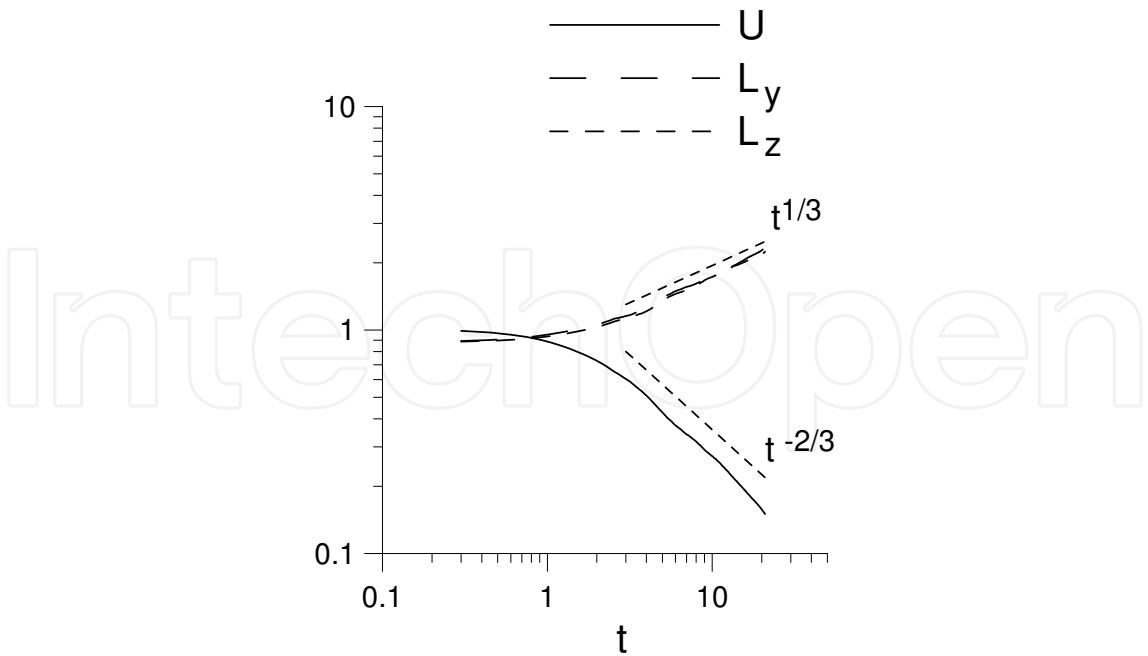


Fig. 2. Temporal development of the velocity and length scales of the non-stratified jet flow.

3. Numerical results

3.1 Jet flow properties

In order to verify the performance of our numerical procedure we performed DNS with  $Re = 700$  of a homogeneous jet flow (where  $Ri = 0$ ) and a stratified jet flow with two different Richardson numbers ( $Ri = 1$  and  $Ri = 3$ ) and compared our numerical results with well-known asymptotics of homogeneous and stratified far wakes.

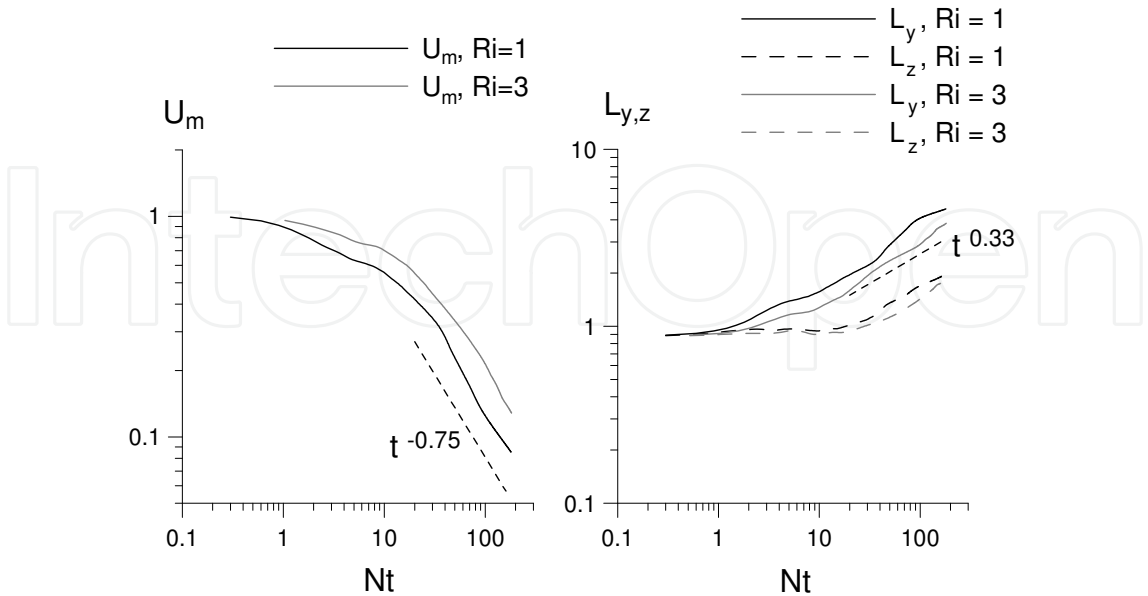


Fig. 3. Temporal development of the jet mean velocity maximum  $U_m$  (left) and its width  $L_y$  and height  $L_z$  (in dashed line) (right). Asymptotics  $U_m \sim t^{-0.75}$  and  $L_{y,z} \sim t^{0.33}$  are shown in dotted line.



Figures 2 and 3 compare the temporal development of the flow integral scales, such as the mean velocity maximum, and jet width and height obtained in our DNS, with the asymptotics  $U_m \sim t^{-2/3}$  and  $U_m \sim t^{-0.75}$  and  $L_{y,z} \sim t^{0.33}$ , observed in homogeneous and stratified wakes in laboratory experiments (Bevilaqua & Lykoudis 1978, Spedding 1997). In the case of a homogeneous wake, the agreement is very good for the considered times  $t \leq 20$  (cf. Fig. 2). (It is important to note that since we normalize by the velocity deficit  $U_0 / V \approx 0.1$ , time moment  $t = 20$  corresponds to the distance  $x / D = tV / U_0 \approx 200$  behind the sphere.) In the stratified case, the agreement with the asymptotics  $U_m \sim t^{-0.75}$  and  $L_{y,z} \sim t^{0.33}$  is also quite satisfactory.

Figure 4 presents the temporal development of the velocity and density fluctuations amplitudes for  $Ri = 1$  and 3. The figure shows that at early times ( $Nt < 10$ ) the velocity fluctuations amplitudes are of the same order, i.e. the flow remains nearly isotropic. At later times, the vertical velocity decreases much faster as compared to the horizontal velocity components and at times  $Nt > 30$  the amplitude  $U'_z$  becomes almost by two orders of magnitude smaller than the horizontal velocity amplitudes  $U'_x$  and  $U'_y$ . Thus, at that stage, the flow becomes quasi-two-dimensional.

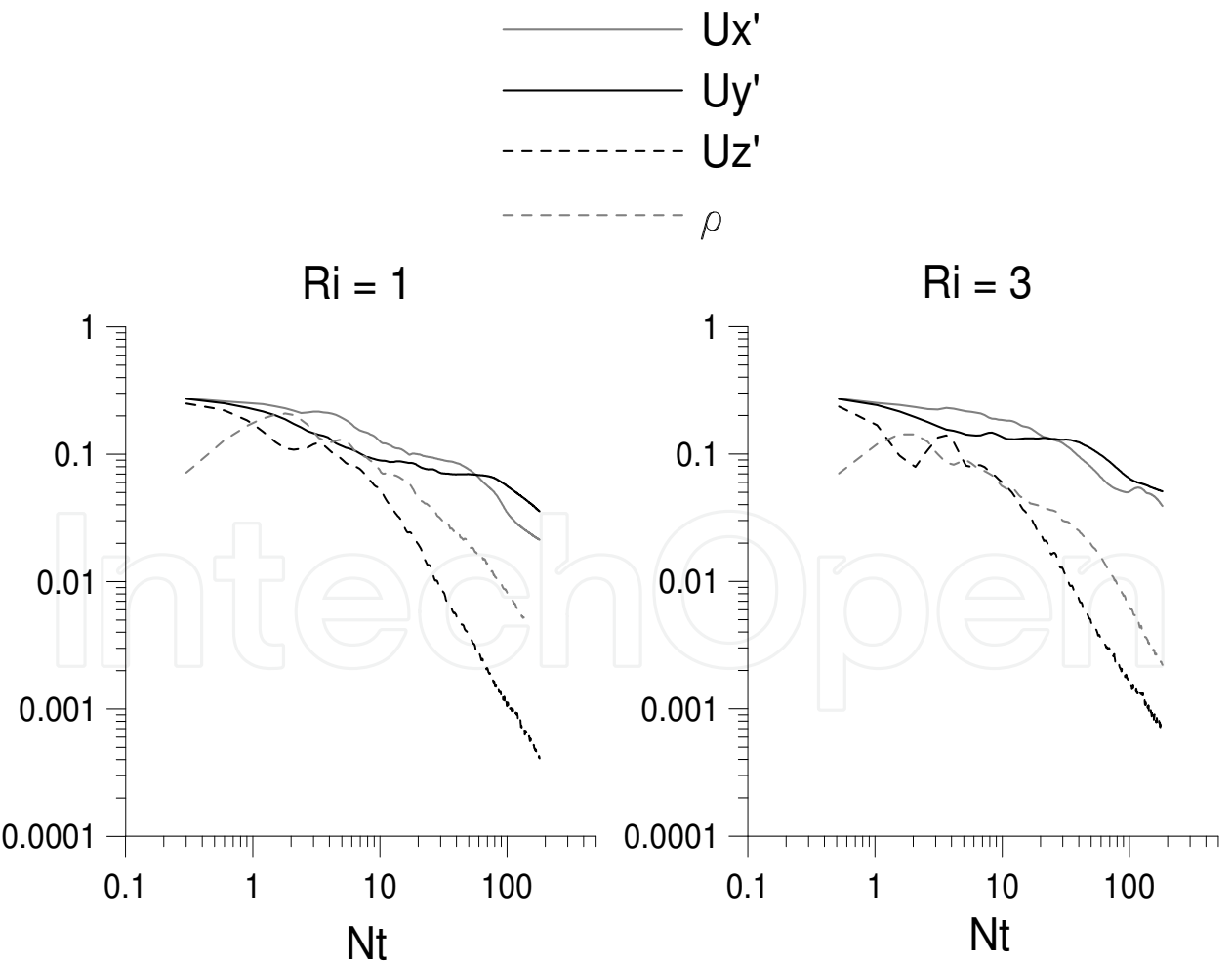


Fig. 4. Temporal development of the velocity and density fluctuations amplitudes for  $Ri = 1$  (left) and  $Ri = 3$  (right).

The density fluctuations amplitude  $\rho'$  increases and reaches its maximum at  $Nt \approx 2$  due to the transfer of the initial turbulence kinetic energy into the potential energy of the displaced isopycnals. Then  $\rho'$  decreases, and this reduction is accompanied by the growth of the vertical velocity fluctuations until  $Nt \approx 3.5$ . At later times the anti-phase oscillations of  $\rho'$  and  $U'_z$  are smeared out due to their decay. Similar behavior was observed by Dommermuth et al. (2002) and interpreted as the radiation of internal waves by collapsing vertical velocity fluctuations in the wake.

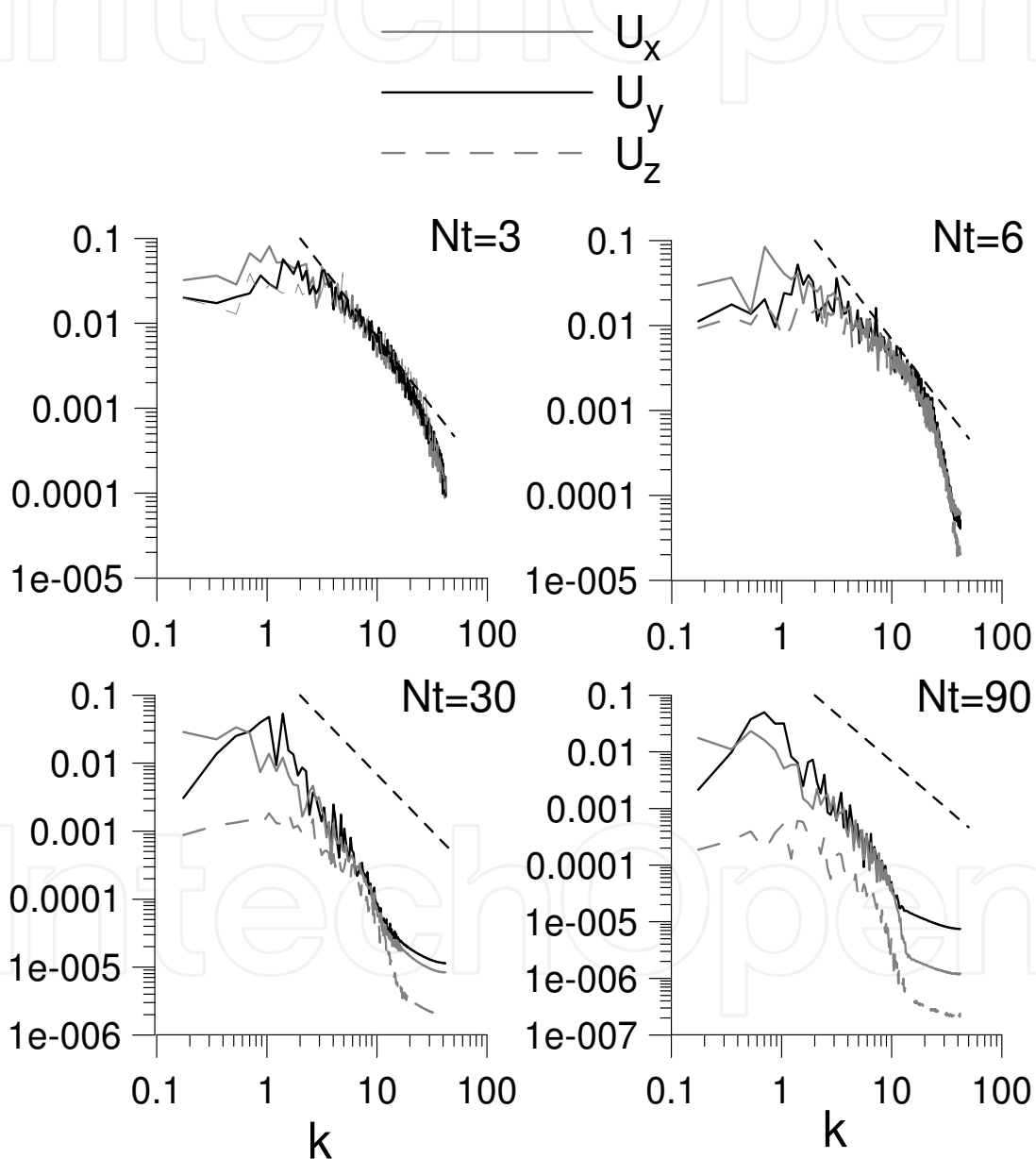


Fig. 5. Velocity fluctuations spatial spectra at different time moments. Asymptotics  $k^{-5/3}$  is shown in dotted line. Here and below in Figs. 6, 7  $Ri = 1$ .

Figure 5 shows the velocity wavenumber spectra  $U_i(k)$  of the  $i = x, y, z$  velocity components obtained in DNS for  $Ri = 1$  at different time moments. Each spectrum is evaluated by a

Fourier transform of the velocity  $i$ -component  $U_i(x, y, z)$  over the streamwise ( $x$ ) coordinate and averaging over 9  $x$ -realizations located in the jet core region  $|y^2 + z^2| < 0.15$ . The figure shows that at early time moments  $Nt = 3, 6$  the spectra  $U_i(k)$  are of the same magnitude, i.e. the velocity field remains isotropic. It is important to note that at these early times the spectra are characterized by distinctive peaks at  $k \approx k_s$  (for  $y$ -component) and  $k \approx 0.5k_s$  (for  $x$ -component) where  $k_s = 1.46$  is the wavenumber of the spiral instability mode of the non-stratified jet flow (Batchelor & Gill 1962). At later times ( $Nt = 30, 90$ ) most of the energy becomes accumulated in the horizontal velocity components  $U_x(k)$  and  $U_y(k)$  with pronounced peaks at  $k \approx 0.5k_s$ .

The dynamics of the spectrum in Fig. 5 can be interpreted as follows. At early times ( $Nt < 10$ ) there occurs a preferential growth of the most unstable mode which, in a certain sense, is analogous to the spiral instability mode of the non-stratified jet flow (Batchelor & Gill 1962). (This is in agreement with numerous experimental observations (cf. e.g. Spedding et al. (1996)) showing that at early times the stratified wake flow develops similarly to the homogeneous wake flow.) It is important to note that this instability mode is an *intrinsic* property of the jet flow itself and is not directly related to the shedding instability mode of the near-wake flow observed experimentally by CBH (1993). It is important to note also that, in our DNS, no selected modes are initially present (cf. Fig. 1). At later times ( $Nt > 30$ ) the flow is governed by the non-linear interaction and competition between the most developed flow modes which leads to the preferential growth of a quasi-2D mode with wavenumber  $0.5k_s$ .

Figure 5 shows also that the fluid kinetic energy is negligible for wavenumbers larger than  $k_{\max} = 20$  (the corresponding spatial scale is  $l_{\min} = 2\pi / k_{\max} \approx 0.3$ ). Thus, for the considered spatial resolution ( $\Delta x = 0.075$ ) the flow, including the smallest scales, is well-resolved in DNS.

Figure 6 presents the instantaneous distribution of the flow vorticity  $z$ -component,  $\omega_z = \partial_x U_y - \partial_y (U_x + U_{ref})$  in the plane  $(x, y)$  at  $z = 0$  obtained in DNS for  $Ri = 1$  at time moments  $Nt = 6$  and  $Nt = 90$ . The figure shows that at late times the vorticity distribution is characterized by the development of large-scale vortices of alternating polarity arranged in the horizontal plane  $(x, y)$  in the vicinity of the jet streamwise axis. Similar vortex structures (also called the “pancake” eddies) are known to be the common feature of stratified far wakes and observed both in laboratory experiments (cf. e.g. Spedding et al. (1996)) and in numerical simulations (Gourlay et al. (2001), Dommermuth et al. (2002)).

It is of interest to note that at times  $30 < Nt < 90$  the amplitude  $U'_y$  of the spanwise fluctuation velocity component remains almost constant whereas the streamwise velocity amplitude,  $U'_x$ , decreases with time, so that at sufficiently late times ( $Nt > 60$ ) the spanwise velocity fluctuations prevail over the streamwise fluctuations (cf. Fig. 4). This behavior of  $U'_y$  and  $U'_x$  is more pronounced for a larger Richardson number (cf. cases  $Ri = 1$  and  $Ri = 3$  in Fig. 4). Figure 5 shows also that at that stage a distinct peak develops in the horizontal velocity spectra  $U_{x,y}(k)$  at wavenumber  $k \approx 0.5k_s$ . This behavior of the spanwise velocity amplitude and the spectrum is in general agreement with the hypothesis put forward by Spedding (2001) who pointed out that an *intrinsic* mean flow sinuous instability may be responsible for the development of the large-scale coherent vortex structures in late stratified wakes.

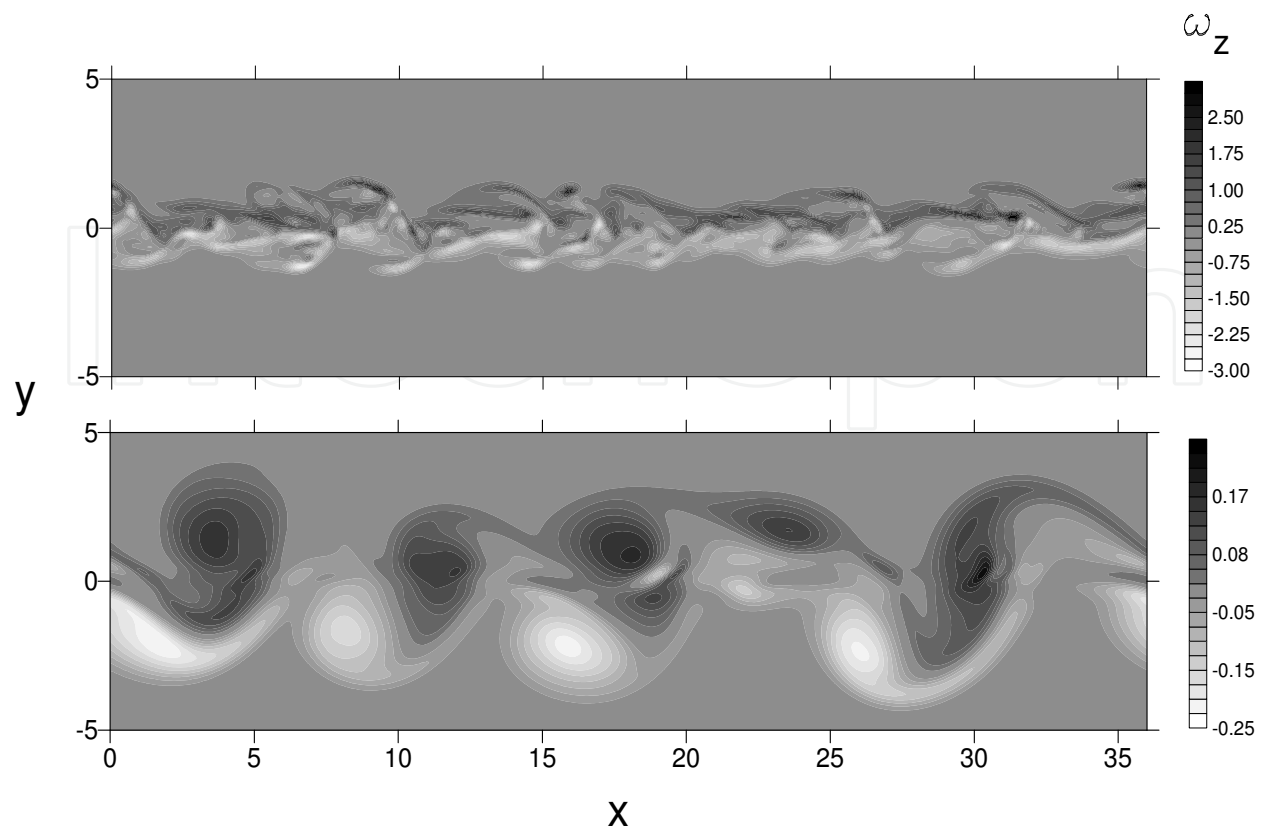


Fig. 6. Instantaneous contours of the vertical vorticity component  $\omega_z$  in the horizontal central  $(x,y)$  plane at time moments  $Nt = 6$  (top frame) and  $Nt = 90$  (bottom frame). The mean flow is from left to right along the  $x$ -axis.

### 3.2 Internal waves radiation

Figure 7 shows the instantaneous distributions of the r.m.s. of the density and horizontal and vertical velocity fields,  $\rho'(y,z)$ ,  $U'_h(y,z) = (U'^2_x + U'^2_y)^{1/2}$  and  $U'_z(y,z)$ , evaluated from (2.15) and (2.16) at different time moments. The figure shows that at sufficiently late times ( $Nt > 10$ ) the vertical velocity fluctuations,  $U'_z(y,z)$ , are mostly present in the region  $|z| > 1$  whereas the horizontal component,  $U'_h(y,z)$ , is most pronounced in a horizontal layer  $|z| < 1$  in the region  $|y| < L_y$ . At times  $Nt = 15, 30$  the vertical velocity fluctuations are most pronounced in the elongated regions oriented at the angle  $\theta$  with respect to the vertical axis in the range  $40^\circ < \theta < 60^\circ$ . It is a well-known property of stratified turbulence that at sufficiently late times, after the initial collapse of 3D turbulence under the action of buoyancy force, the vertical velocity is associated mostly with propagating internal waves (IW) whereas the horizontal velocity is associated with quasi-2D fluid motions. Fig. 7 shows that at later times ( $Nt = 60, 90$ ) amplitude  $U'_z$  decreases by the order of magnitude as compared to the time moment  $Nt = 15$ , and the regions of local maxima of  $U'_z(y,z)$  are getting aligned with the vertical axis. This picture is similar to the one predicted by a linear theory for the IW radiated by an impulsive point source (Zavolski & Zaytsev 1984, Voisin 1991). According to this theory, amplitude of IW emitted impulsively by a point source has its maximum along the iso-phase line oriented at  $\theta = \arctan \sqrt{2} \approx 55^\circ$  with respect to the

vertical. At later times, at a given point, IW cancel out due to their mutual destructive interference and are superceded by small-amplitude, non-propagating buoyancy oscillations. (Below we discuss the application of the impulsive point theory in the considered case in more detail.)

Figure 7 shows also that the distribution of the density fluctuation in the vicinity of the jet core has a two-layer structure with local maxima of  $\rho'$  at  $|z| \approx 0.5$ ,  $y \approx \pm 2$ . Now it is well known that the fluid density variations in a pancake vortex arise as a result of the cyclostrophic balance, where the centrifugal force inside the vortex is balanced by a vertical pressure gradient force that is provided by a perturbation of the local density (cf. Beckers et al. (2001)). This balance inside the individual vortex deflects isopycnals toward the vortex center and thus creates a two-layer distribution of the local density perturbation. Figure 6 shows that the centers of pancake vortices are located in the horizontal central plane at  $y \approx \pm 2$ . Thus it is plausible to assume that the local maxima of  $\rho'$  at  $|z| \approx 0.5$ ,  $y \approx \pm 2$  in the distribution of the density fluctuation (cf. Fig. 7,  $Nt = 60, 90$ ) are due to the cyclostrophic balance inside the pancake eddies.

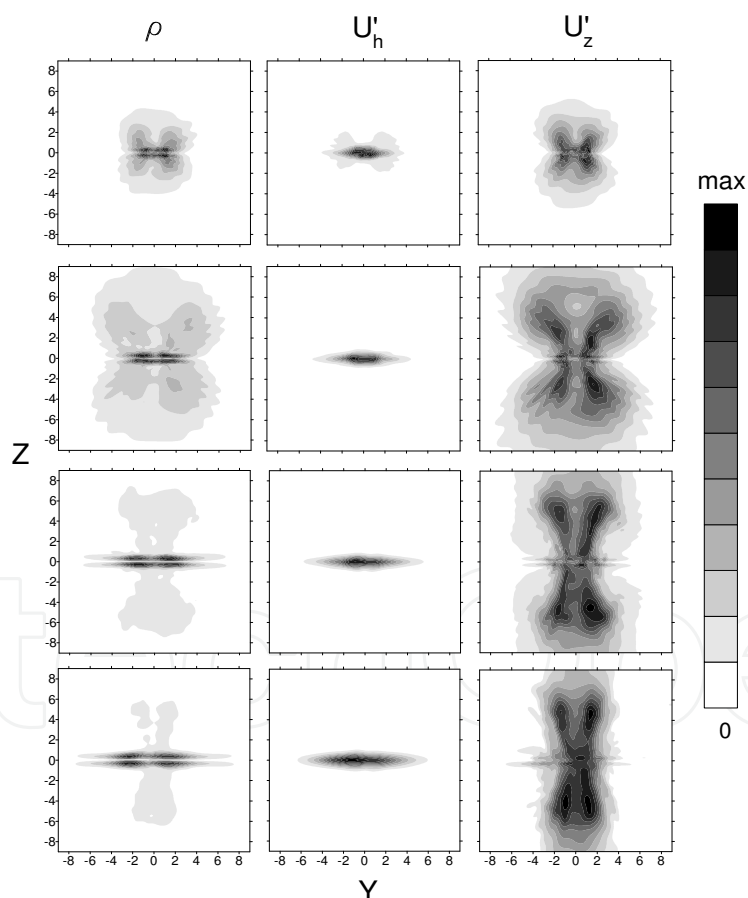


Fig. 7. Contours of the  $x$ -averaged density fluctuation  $\rho$  (left column), and horizontal (centre column) and vertical (right column) velocity fluctuations,  $U'_h$  and  $U'_z$ , obtained at time moments  $Nt = 15, 30, 60, 90$  (from top to bottom). The respective maximum values are: 0.06, 0.12, 0.028 ( $Nt = 15$ ); 0.03, 0.1, 0.0085 ( $Nt = 30$ ); 0.016, 0.09, 0.0028 ( $Nt = 60$ ); 0.0095, 0.07, 0.0012 ( $Nt = 90$ ).

Figure 8 shows the instantaneous distribution of the vertical velocity component,  $U_z$ , in the vertical  $(x, z)$  planes at  $y = 0$  and  $y = 1.5$  obtained in DNS at time moments  $Nt = 15$  and  $Nt = 90$ . The figure shows that at time moment  $Nt = 15$ , in the region sufficiently far away from the jet streamwise axis (for  $|z| > 1$ ), IW isophase lines, which are associated with the regions of maxima and minima of  $U_z$ , are mostly in the direction of the mean flow and oriented at the angle of  $\theta \approx 50^\circ$  with respect to the vertical. The velocity distribution has a nearly periodical spatial structure with a period of about 5 dimensionless units along the  $x$ -coordinate. The figure shows also that at time  $Nt = 90$  the vertical velocity amplitude is diminished by the order of magnitude and its maxima and minima are arranged in columns with the same spatial periodicity. These maxima and minima can be associated with small-amplitude buoyancy oscillations which supercede impulsively radiated IW at that stage of the flow development (Voisin 1991).

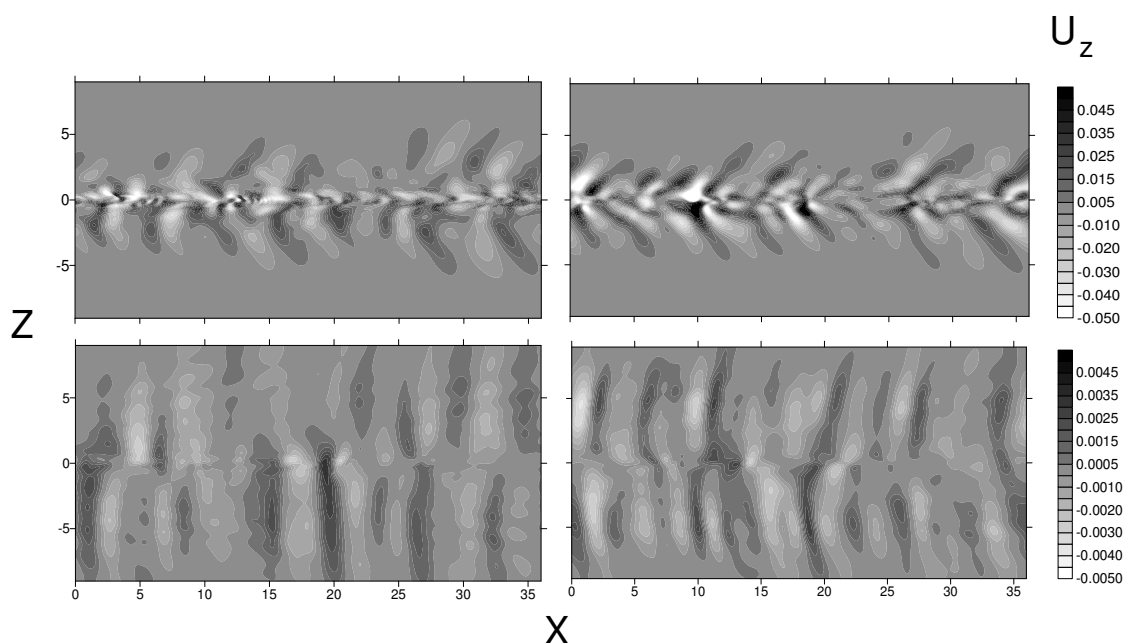


Fig. 8. Instantaneous contours of the vertical velocity  $U_z$  in the vertical  $(x, z)$  plane at  $y = 0$  (left column) and  $y = 1.5$  (right column) at time moments  $Nt = 15$  (top frame) and  $Nt = 90$  (bottom frame).

Figure 9 presents the distribution of the vertical velocity,  $U_z$ , in the horizontal  $(x, y)$ -plane at the distance  $z = 3$  above the jet streamwise axis obtained in DNS at time moments  $Nt = 12, 15, 18$ . The figure shows that the IW patterns in that plane are similar to the IW patterns of stationary lee-waves and characterized by a well-defined streamwise spatial period of about 5 dimensionless units (or about 4-5 sphere diameters in the dimensional form). A similar isophase pattern was observed by BCH in the laboratory experiment in a horizontal plane at a distance of three sphere radii away from the towing axis. Note also that this spatial period is close to the wavelength of the spiral instability mode of the non-stratified jet flow  $\lambda_s = 2\pi / k_s \approx 4.3$  for  $k_s \approx 1.46$  (Batchelor and Gill 1962).

Figure 10 shows the temporal development of the vertical velocity and density,  $U_z$  and  $\rho$ , obtained in DNS at the point located at  $x = 18$ , with the angle with respect to the vertical  $\theta =$



$40^\circ$  at the distance of  $|y^2 + z^2| = 3$  from the jet streamwise axis for Richardson numbers  $Ri = 1$  and  $Ri = 3$ . The figure shows that in both cases IW packet arrives at the observation point at time moment  $Nt \approx 10$  which is independent of the Richardson number. At the given point, the IW packet amplitude grows at times  $Nt < 20$  whereas the velocity  $U_z$  and density  $\rho$  oscillate with a phase shift  $\pi/2$  typical of a monochromatic, linear internal wave (Phillips 1977). At times  $Nt > 30$  the oscillations of  $U_z$  and  $\rho$  become incoherent and IW packet amplitude decreases. At sufficiently late times ( $Nt > 60$ ) there remain only small-amplitude oscillations of the velocity and density with the buoyancy frequency  $N$ . These small-amplitude oscillations are similar to the buoyancy oscillations which supercede internal waves, which are mutually cancelled due to the destructive interference as their wavelengths become of the order of the source diameter (i.e. of order one in the considered case) (Voisin 1991).

Figure 11 presents spatially averaged frequency spectra of the vertical velocity obtained in DNS for Richardson numbers  $Ri = 1$  and  $3$ . Each spectrum was obtained by Fourier transform of time series  $U_z(t)$  and averaged over 100 points located uniformly at a cylindrical surface with radius  $|y^2 + z^2| = 3$  in the range  $0^\circ < \theta < 90^\circ$ . The figure shows that the velocity spectra are characterized by a well pronounced peak at the frequency  $\omega/N \approx 0.7$  which corresponds to the IW propagation angle  $\arccos \omega/N \approx 45^\circ$ . This value is close to the prediction of the linear theory stating that the amplitude of the waves radiated impulsively by a small-size source has a maximum at  $\theta = \arctan \sqrt{2} \approx 55^\circ$ . This is also in general agreement with the data in Figs. 7 and 8 discussed above.

Figure 12 presents the dependence of the internal waves amplitude ( $\rho_{iw}$ ) vs. the inverse Richardson number ( $Ri^{-1}$ ) obtained in DNS for two different values of the Reynolds number,  $Re = 400$  and  $700$ . The IW amplitude was evaluated in each DNS run as a maximum of the r.m.s. density fluctuation  $\rho'(y, z, t)$  (2.16) at the distance  $|y^2 + z^2| = 3$  from the jet streamwise axis. (Note that since we consider the linear reference density profile,  $\rho'(y, z, t)$  is also equivalent to the average fluid particle vertical displacement amplitude i.e. the average IW amplitude.). The DNS results show that, for all considered  $Ri$ , the maximum of  $\rho'$  is observed at time moment  $Nt \approx 15$  in the range  $40^\circ < \theta < 60^\circ$ . Figure 12 shows that IW amplitude decreases with increasing  $Ri$ . The figure also shows an asymptotic estimate for the amplitude of the impulsively emitted internal waves (in dotted line).

Below in Section 4 the application of the impulsive source theory to explain the observed IW kinematics and dynamics is discussed.

#### 4. Impulsive source model

Radiation of internal waves by the jet turbulence occurs due to the transfer of the kinetic energy of the vertical velocity fluctuations into the initial potential energy of isopycnal displacement and its further redistribution between the kinetic and potential energy of waves and turbulence. This transfer is most pronounced at the early stage of the jet flow evolution when the vertical velocity fluctuations are significant (i.e. for  $Nt < 10$ , cf. Fig. 4). The results in the previous section show that the properties of IW radiated by the jet flow turbulence are to some degree analogous to the properties of the internal waves radiated by an impulsive source. Let us consider this analogy in more detail.

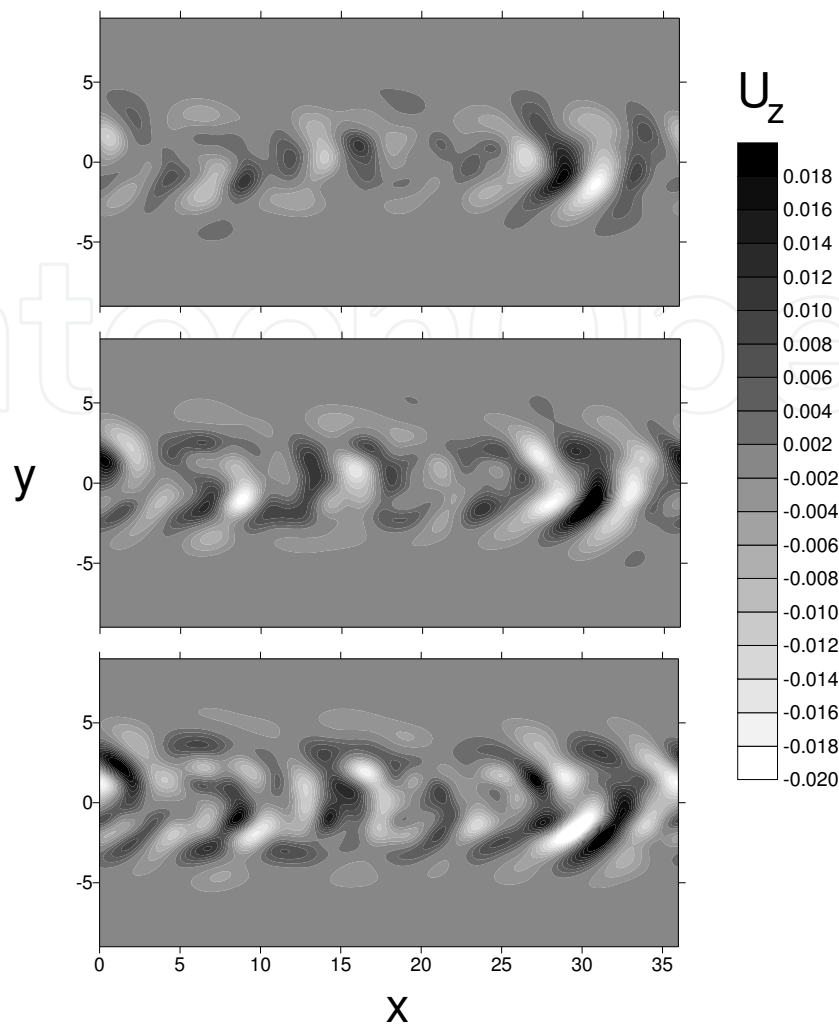


Fig. 9. Instantaneous contours of the vertical velocity  $U_z$  in the horizontal  $(x, y)$  plane above the jet streamwise axis at  $z = 3$  at time moments  $Nt = 12, 15, 18$  (from top to bottom).

In the considered case, an IW radiation source function can be evaluated from the equation for the vertical velocity derived by Phillips (1977). In this equation, the non-linear terms are not discarded but can be regarded as an effective source of IW. This equation is derived in the inviscid case in the form:

$$\frac{\partial^2}{\partial t^2}(\nabla^2 U_z) + N^2 \nabla_h^2 U_z = Q(x, y, z, t) \quad (4.1)$$

where the IW source function is

$$Q(x, y, z, t) = \frac{\partial^3}{\partial x_\alpha \partial z \partial t} \left( U_j \frac{\partial U_\alpha}{\partial x_j} \right) - \nabla_h^2 \left\{ U_j \frac{\partial b}{\partial x_j} + \frac{\partial}{\partial t} \left( U_j \frac{\partial U_z}{\partial x_j} \right) \right\} \quad (4.2)$$

In (4.1) and (4.2) the notations are as follows:  $\nabla^2 \equiv \frac{\partial^2}{\partial x^2} + \frac{\partial^2}{\partial y^2} + \frac{\partial^2}{\partial z^2}$ ,  $\nabla_h^2 \equiv \frac{\partial^2}{\partial x^2} + \frac{\partial^2}{\partial y^2}$  are the full and horizontal Laplasian operators, respectively; summation over the repeated indexes

$\alpha = 1, 2$  and  $j = 1, 2, 3$  is performed;  $(x_1, x_2, x_3) \equiv (x, y, z)$  are the Cartesian coordinates;  $(U_1, U_2, U_3) \equiv (U_x, U_y, U_z)$  are the fluid velocity components; and  $b = -Ri\rho$  is the buoyancy.

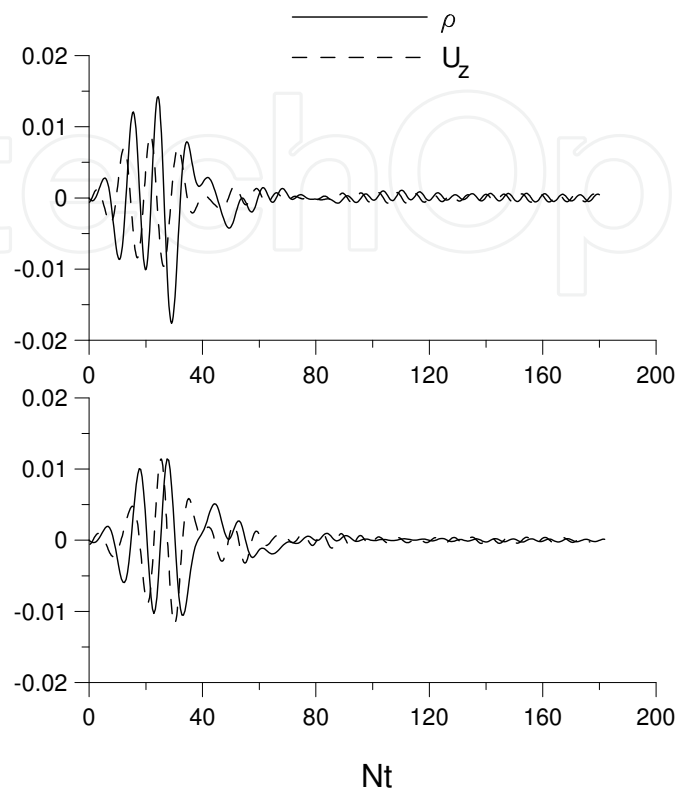


Fig. 10. Temporal development of the vertical velocity and density,  $U_z$  and  $\rho$ , obtained in DNS at  $x = 18$  and  $\theta = 40^\circ$  (the angle with respect to the vertical) at the distance  $|y^2 + z^2| = 3$  from the jet streamwise axis for Richardson numbers  $Ri = 1$  (top frame) and  $Ri = 3$  (bottom frame).

Figure 13 shows an instantaneous distribution of the source function  $Q(x, z, y = 0)$  evaluated in DNS in the central vertical plane at time moments  $Nt = 3$  and 6. The figure shows that the distribution of  $Q$  is quite inhomogeneous and confined to the jet core region. Therefore, the effective source diameter is of the order of the initial jet flow diameter. The figure indicates also that the growth of the modes with wavenumbers  $k \approx k_s$  and  $k \approx 0.5k_s$  in the velocity spectra at time moments  $Nt < 10$  (Fig. 5) leads to a modulation of the source function amplitude along the streamwise coordinate. (In Fig. 13 this modulation is more pronounced at time moment  $Nt = 6$ .)

Figure 14 presents the temporal development of the volume-averaged dispersion of the IW source function,  $\langle Q(x, y, z, t)^2 \rangle^{1/2}$ , obtained in DNS for  $Ri = 1$  and  $Ri = 3$ . The figure shows that, for all  $Ri$ , the dispersion increases by  $t = 2.5$  by the order of magnitude. The figure shows also that at later times  $\langle Q(x, y, z, t)^2 \rangle^{1/2}$  decays, so that its amplitude is reduced by more than half by  $t = 5$  and becomes negligible at  $Nt > 10$ . From the spectra in Fig. 11 the period of internal waves having the maximum amplitude can be evaluated as  $NT_{IW} = 2\pi N / \omega \approx 8$  (cf. Fig. 11) and is almost twice as large as compared to the period of the IW source function half-decay.

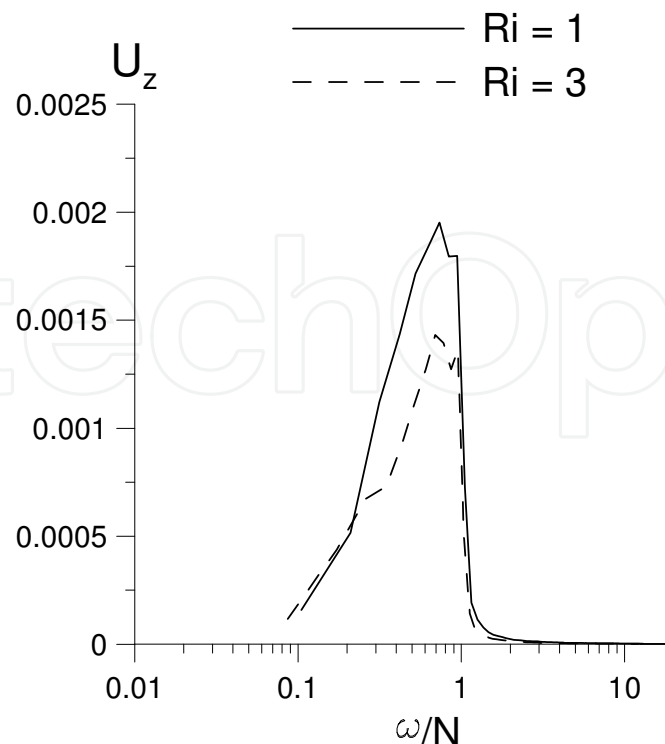


Fig. 11. Spatially averaged frequency spectra of the vertical velocity obtained in DNS for different Richardson numbers.

Thus  $Q$  in (4.1) can be regarded as an impulsive source function which brings about IW radiation by the jet flow turbulence. The temporal growth and maximum amplitude of this source function is controlled by the non-linear flow dynamics, not by buoyancy. Let us now make some estimates provided by the impulsive source theory (Zavolskii & Zaytsev 1984, Voisin 1991, BCH 1993) concerning the kinematics and dynamics of the radiated internal waves.

The time interval during which the IW packet, emitted impulsively by the source (S) at the angle  $\theta$  with respect to the vertical (cf. Fig. 15), comes to the observation point (O) located at the distance  $r = \sqrt{y^2 + z^2}$ , can be estimated with the use of the linear theory as follows. The group velocity ( $c_g$ ) of internal waves with streamwise wavenumber  $k$  and the isophase line at the angle  $\theta$  with respect to the vertical is evaluated as:

$$c_g = \frac{N}{2k} \sin 2\theta. \quad (4.3)$$

Thus the time interval,  $Nt_1$ , during which the IW wave packet comes from the source (S) to the observation point (O), is evaluated as:

$$Nt_1 = \frac{2kr}{\sin 2\theta}. \quad (4.4)$$

Eq. (4.4) shows that time interval  $Nt_1$  does not depend on  $N$  in agreement with the DNS results in Fig. 10. Substitution of  $r = 3$ ,  $\theta = \arctan \sqrt{2}$ , and  $k = k_s \approx 1.3$  into (4.4) gives the estimate  $Nt_1 \approx 8$ , which is also in good agreement with the DNS results in Fig. 10.

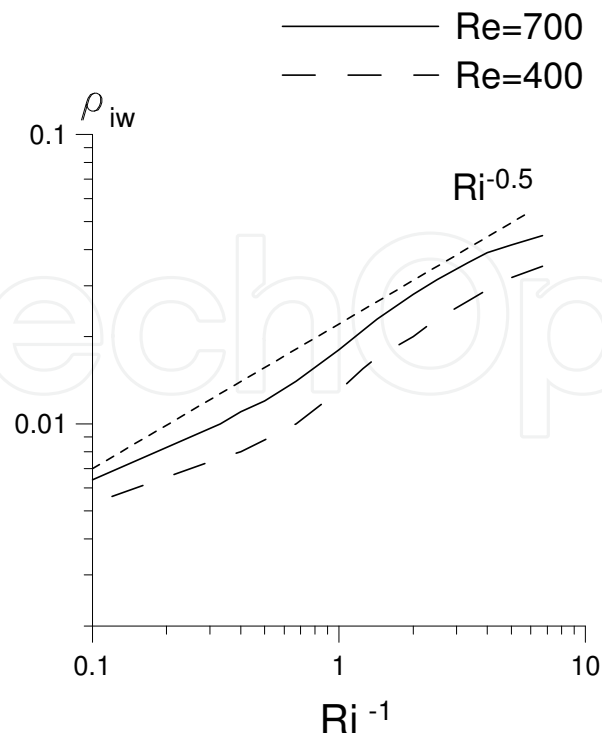


Fig. 12. The internal waves amplitude ( $\rho_{iw}$ ) vs. inverse Richardson number obtained in DNS for different Reynolds numbers. The dotted line shows the asymptotic solution for the amplitude derived from the linear theory for an impulsive point source.

Figure 10 shows that at sufficiently late times ( $Nt > 40$ ) the density oscillations at the considered distance from the jet streamwise axis ( $r = 3$ ) are damped. The time moment ( $Nt_2$ ) after which the IW amplitude decays at a given location can be estimated as follows. The wavelength  $\lambda$  of IW emitted impulsively by a source (S) at the angle  $\theta$  with respect to the vertical at the distance  $r$  and coming to the observation point (O) at time  $t$  (cf. Fig. 15) can be evaluated as:

$$\lambda \approx \frac{2\pi r}{Nt \sin \theta} \quad (4.5)$$

The theoretical analysis of the internal waves field generated by a sphere performed by Voisin (1994) shows that if  $\lambda$  becomes of the order of the sphere radius, the destructive interference of the waves emitted from different locations on the sphere leads to a decay of the wave amplitude. In the considered case, the cutoff wavelength is of the order of the jet initial diameter, i.e.  $\lambda_c \approx 1$ . Substitution of  $\lambda = \lambda_c$  in (4.5) gives

$$Nt_2 \approx \frac{2\pi r}{\sin \theta} \quad (4.6)$$

For  $r = 3$  and  $\theta = \arctan \sqrt{2}$  we obtain from (4.6) an estimate  $Nt_2 \approx 30$ , which is also in good agreement with the DNS results (Fig. 10). The linear theory also predicts that at times  $Nt \gg Nt_2$ , the incoming waves are mutually cancelled, and there remain only buoyancy

oscillations of the density with the frequency  $N$  whose group velocity is identically zero. These buoyancy oscillations are present in Fig. 10 (for  $Nt > 40$ ) and in the distributions of the vertical velocity in the form of columnar disturbances at time moment  $Nt = 90$  in Figs. 7, 8. The asymptotics for the IW amplitude in Fig. 12 is derived as follows. Using the same schematic in Fig. 15 the following estimate can be obtained for the amplitude of internal waves ( $\rho_{iw}$ ) emitted impulsively by the source (S) and coming to the observation point (O) at time  $t$  (cf. e.g. BCH):

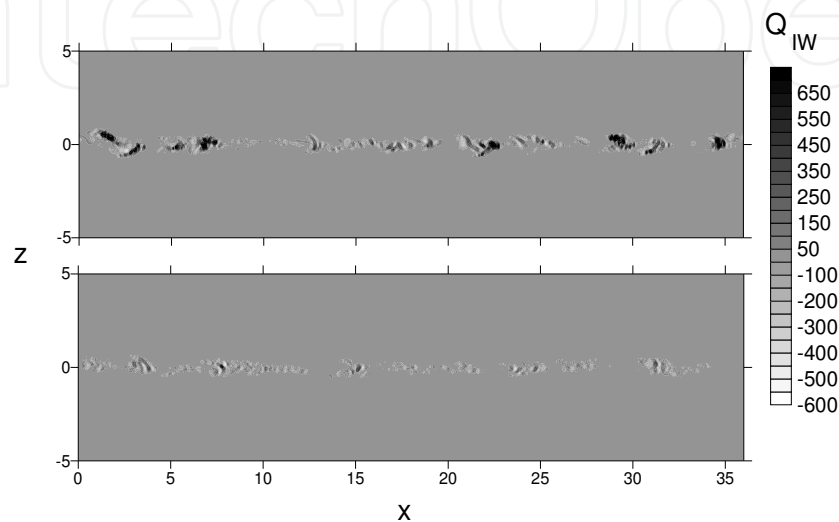


Fig. 13. Instantaneous contours of the IW source function  $Q_{IW}$  in the vertical central plane at time moments  $Nt = 3$  (top frame) and  $Nt = 6$  (bottom frame).

$$\rho_{iw} \sim \frac{\sin \theta [Nt |\cos \theta|]^{1/2}}{Nr}. \quad (4.7)$$

Eq. (4.7) shows that  $\rho_{iw}$  increases with time. As it was discussed above, the IW amplitude increases until time when the wavelength of incoming waves becomes of the order of the source size, i.e. for  $Nt \leq Nt_2$ . Thus, the maximum amplitude ( $\rho_{iw}^{\max}$ ) can be evaluated from (4.6) and (4.7) as:

$$\rho_{iw}^{\max} \sim \frac{[\pi |\sin 2\theta|]^{1/2}}{Nr^{1/2}}. \quad (4.8)$$

Eq. (4.8) shows that IW amplitude is inversely proportional to  $N$ , so that  $\rho_{iw}^{\max} \sim Ri^{-0.5}$ . (Note that the jet flow Froude number equals  $Fr_j = 1 / \sqrt{Ri}$ , so that  $\rho_{iw}^{\max} \sim Fr_j$ .) This estimate is in good agreement with the results in Fig. 12 for sufficiently small amplitudes (for  $\rho_{iw} < 0.03$ ). The growth of  $\rho_{iw}$  saturates for larger amplitudes, probably due to nonlinear effects, and increases for larger Reynolds number.

## 5. Conclusions and discussion

In the present paper, direct numerical simulation (DNS) has been performed in order to study the process of internal waves radiation by a stratified turbulent jet flow. An initially



circular, turbulent jet flow with a Gaussian profile of the mean streamwise velocity component in a fluid with stable, linear density stratification is considered which models the flow created in the far wake of a sphere towed in a stratified fluid at large Froude and Reynolds numbers. The DNS results show that at early times ( $Nt < 30$ , where  $N$  is the buoyancy frequency) there occurs a collapse of the vertical velocity fluctuations which brings about the radiation of internal waves (IW). The characteristic spatial period of these waves is found to be close to the wavelength of the spiral instability mode of a non-stratified jet flow. The IW amplitude decreases with increasing the flow global Richardson number and is well described by the asymptotics  $\rho_{iw} \sim Ri^{-0.5}$ . At late times ( $Nt > 60$ ) the jet flow becomes quasi-two-dimensional and is dominated by large-scale pancake vortices. At that stage, internal waves are superseded by non-propagating, columnar, small-amplitude buoyancy oscillations confined to a central vertical layer with a thickness of the order of the jet width. A linear model is proposed where the jet turbulence collapsing under the stabilizing effect of the buoyancy forces, is regarded as an impulsive source of IW radiation. The kinematics and dynamics of the internal waves observed in DNS are found to be in good agreement with the model prediction.

Note that a relatively narrow IW frequency range ( $40^\circ < \arccos \omega / N < 60^\circ$ ), similar to the one observed in our DNS, has been also observed in mixing-box experiments (Dohan & Sutherland 2003), in a flow over a vertical obstacle (Sutherland & Linden 1998), during the collapse of a mixed patch (Sutherland et al. 2007) and in LES of a density-stratified boundary layer (Taylor & Sarkar 2007). In these works, several models were proposed to explain the observed IW frequency range, and among them, perhaps, two pertain to the considered case of IW radiation by a temporally developing turbulent jet flow. Dohan and Sutherland (2003) employed stability criteria derived by Sutherland (2001) for low- and high-frequency waves which show that the largest critical IW amplitude corresponds to the waves propagating at  $\theta = 45^\circ$ .

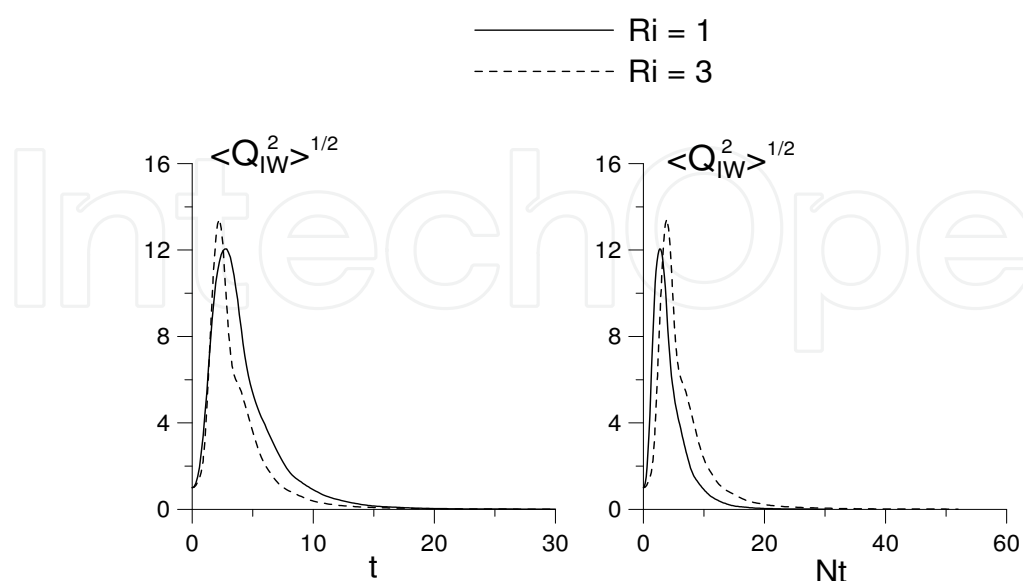


Fig. 14. Temporal development of the volume-averaged dispersion of the IW source function normalized by its initial value for different Richardson numbers. Note that the graph on the right is scaled with the buoyancy frequency.

Other waves become unstable at a lower amplitude and their breaking would explain the observed frequency selection. However, in our case the wave amplitude is much smaller than the critical value  $A_{IW} / \lambda_x \approx 0.07$  (cf. Fig. 4 where  $\rho_{\max}^{IW} \approx 0.05$  and  $\rho_{\max}^{IW} / \lambda_x < 0.01$  for  $\lambda_x \approx 5$ ) and this mechanism is not applicable. Taylor and Sarkar (2007) developed a linear viscous model to estimate the decay in wave amplitude. Waves with high and low frequencies have smaller vertical group velocities and dissipate more as compared to the waves with propagation angle in the vicinity of  $\theta \approx 27^\circ$ . Thus the viscous dissipation may cause the observed selected IW frequency range. However, our DNS results show that the selection of the IW propagation angle occurs in the close vicinity of the jet core region ( $|z| > 1$ ) where viscous diffusion effects have not yet accumulated and are negligible as far as the frequency selection is concerned. Therefore, the impulsive source model considered in the present paper provides the most plausible explanation of the IW kinematics and dynamics observed in DNS.

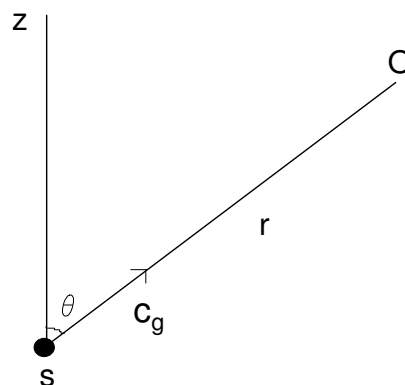


Fig. 15. Schematic of the radiation of the IW packet by an impulsive point source (S) with the group velocity  $c_g$  at the angle  $\theta$  with respect to the vertical axis at the distance  $r$  from the observation point (O).

## 6. Acknowledgement

This work is supported by RFBR (10-05-00339, 10-05-91177, 09-05-00779, 11-05-00455, 10-01-00435).

## 7. References

- Batchelor J.K. & Gill A.E. (1962). Analysis of the stability of axisymmetric jets. *J. Fluid Mech.* Vol. 14, pp. 559-551.
- Beckers M., Verzicco R., Clercx H.J.H., & Van Heist G.J.F. (2001) Dynamics of pancake-like vortices in a stratified fluid: experiments, model and numerical simulations. *J. Fluid Mech.* Vol. 433, pp. 1-27.
- Bevilaqua P.M. and Lykoudis P.S. (1978). Turbulence memory in self-preserving wakes. *J. Fluid Mech.* Vol. 89, pp. 589-606.
- Bonneton P., Chomaz J.M., & Hopfinger E.J. (1993). Internal waves produced by the turbulent wake of a sphere moving horizontally in a stratified fluid. *J. Fluid Mech.* Vol. 254, pp. 23-40.

- Brucker K.A. & Sarkar S. (2010a). A comparative study of self-propelled and towed wakes in a stratified fluid. *J. Fluid Mech.* Vol. 652, p. 373. Chomaz J.M., Bonneton P., & Hopfinger E.J. (1993). The structure of the near wake of a sphere moving horizontally in a stratified fluid. *J. Fluid Mech.* Vol. 254, pp. 1-21.
- Dohan K. & Sutherland B.R. (2003). Internal waves generated from a turbulent mixed region. *Phys. Fluids* Vol. 15, pp. 488-498.
- Dommermuth D.G., Rottman J.W., Innis G.E., & Novikov E.A. (2002). Numerical simulation of the wake of a towed sphere in a weakly stratified fluid. *J. Fluid. Mech.* Vol. 437, pp. 83-101.
- Druzhinin O.A. (2009). Generation of Internal Waves by a Turbulent Jet in a Stratified Fluid. *Fluid Dynamics*, Vol. 44, No. 2, pp. 213-223.
- Dupont P. & Voisin B. (1996). Internal waves generated by a translating and oscillating sphere. *Dyn. Atm. Oceans*. Vol. 23, pp. 289 - 298.
- Gerz T., Shumann U., & Elghobashi S.E. (1989). Direct numerical simulation of stratified homogeneous turbulent shear flows. *J. Fluid Mech.* Vol 200, pp. 563-594.
- Gourlay M.J., Arendt S.C., Fritts D.C., & Werne J. (2001). Numerical modeling of initially turbulent wakes with net momentum. *Phys. Fluids*. Vol. 13, pp. 3783-3802.
- Javam A., Imberger J. & Armfield S.W. (2000). Numerical study of internal wave-wave interactions in a stratified fluid. *J. Fluid Mech.* Vol. 415, pp. 65-87.
- Lin J.T. & Pao Y.H. (1979). Wakes in stratified fluid. *Annu. Rev. Fluid Mech.* Vol. 11, pp. 317-338.
- Michalke A. & Hermann G. (1982) On the inviscid instability of a circular jet with external flow. *J. Fluid Mech.* Vol. 114, pp. 343-359 .
- Phillips O.M. (1977). *Dynamics of the upper ocean*. 2<sup>nd</sup> ed. Cambridge Univ. Press.
- Plaschko P. (1979). Helical instabilities of slowly divergent jets. *J. Fluid Mech.* Vol. 92, Part 2, pp. 209-215.
- Spedding G.R. (1997). The evolution of initially turbulent bluff-body wakes at high internal Froude number. *J. Fluid Mech.* Vol. 337, pp. 283-301.
- Spedding G.R. (2001). Anisotropy in turbulence profiles of stratified wakes. *Phys. Fluids*. Vol.13, pp. 2361-2372. Spedding G.R., Browand F.K., & Fincham A.M. (1996). Turbulence, similarity scaling and vortex geometry in the wake of a towed sphere in a stably stratified fluid. *J. Fluid Mech.* Vol. 314, pp. 53-103.
- Stadler M.B., Sarkar S. & Brucker K.A. (2010). Effect of the Prandtl number on a stratified turbulent wake. *Physics of Fluids*. Vol. 22, p. 095102.
- Sutherland B.R. & Peltier W.R. (1994). Turbulence transition and internal wave generation in density stratified jets. *Phys.Fluids*. Vol.6, pp. 1267-1284.
- Sutherland B.R. & Linden P.F. (1998). Internal waves excitation from stratified flow over a thin barrier. *J. Fluid Mech.* Vol. 377, pp. 223-252.
- Sutherland B.R. (2001). Finite-amplitude internal wavepacket dispersion and breaking. *J. Fluid Mech.* Vol. 429, pp. 343-380.
- Sutherland B.R., Chow A.N.F., & Pittman T.P. (2007). The collapse of a mixed patch in stratified fluid. *Phys. Fluids* Vol.19, pp. 116602-1-6.
- Taylor J.R. & Sarkar S. (2007). Internal gravity waves generated by a turbulent bottom Ekman layer. *J. Fluid Mech.* Vol. 590, pp. 331-354.
- Voisin B. (1991). Internal wave generation in uniformly stratified fluids. Part 1. Green's function and point sources. *J.Fluid Mech.* Vol. 231, pp. 439-480.
- Zavolski N.A. & Zaitsev A.A. (1984). Development of internal waves generated by a concentrated pulse source in an infinite uniformly stratified fluid. *J. Appl. Mech. Tech. Phys.* Vol. 25, pp. 862-867.



## Computational Simulations and Applications

Edited by Dr. Jianping Zhu

ISBN 978-953-307-430-6

Hard cover, 560 pages

**Publisher** InTech

**Published online** 26, October, 2011

**Published in print edition** October, 2011

The purpose of this book is to introduce researchers and graduate students to a broad range of applications of computational simulations, with a particular emphasis on those involving computational fluid dynamics (CFD) simulations. The book is divided into three parts: Part I covers some basic research topics and development in numerical algorithms for CFD simulations, including Reynolds stress transport modeling, central difference schemes for convection-diffusion equations, and flow simulations involving simple geometries such as a flat plate or a vertical channel. Part II covers a variety of important applications in which CFD simulations play a crucial role, including combustion process and automobile engine design, fluid heat exchange, airborne contaminant dispersion over buildings and atmospheric flow around a re-entry capsule, gas-solid two phase flow in long pipes, free surface flow around a ship hull, and hydrodynamic analysis of electrochemical cells. Part III covers applications of non-CFD based computational simulations, including atmospheric optical communications, climate system simulations, porous media flow, combustion, solidification, and sound field simulations for optimal acoustic effects.

### How to reference

In order to correctly reference this scholarly work, feel free to copy and paste the following:

Oleg Druzhinin (2011). Internal Waves Radiation by a Turbulent Jet Flow in a Stratified Fluid, Computational Simulations and Applications, Dr. Jianping Zhu (Ed.), ISBN: 978-953-307-430-6, InTech, Available from: <http://www.intechopen.com/books/computational-simulations-and-applications/internal-waves-radiation-by-a-turbulent-jet-flow-in-a-stratified-fluid>

**INTeCH**  
open science | open minds

#### InTech Europe

University Campus STeP Ri  
Slavka Krautzeka 83/A  
51000 Rijeka, Croatia  
Phone: +385 (51) 770 447  
Fax: +385 (51) 686 166  
[www.intechopen.com](http://www.intechopen.com)

#### InTech China

Unit 405, Office Block, Hotel Equatorial Shanghai  
No.65, Yan An Road (West), Shanghai, 200040, China  
中国上海市延安西路65号上海国际贵都大饭店办公楼405单元  
Phone: +86-21-62489820  
Fax: +86-21-62489821

© 2011 The Author(s). Licensee IntechOpen. This is an open access article distributed under the terms of the [Creative Commons Attribution 3.0 License](https://creativecommons.org/licenses/by/3.0/), which permits unrestricted use, distribution, and reproduction in any medium, provided the original work is properly cited.

IntechOpen

IntechOpen